Facile and One-Pot Photochemical Synthesis of Highly Conductive PEDOT:PSS: Towards Sustainable and Durable Supercapacitors

Yusra Bahar Cakir , Nahid Keshtiban , Fatih Can Sarı , Ali Gelir , Kerem Kaya *

Posted Date: 2 December 2025

doi: 10.20944/preprints202512.0183.v1

Keywords: conductive polymers; PEDOT:PSS; photopolymerization; energy storage; supercapacitors

 doi:10.20944/preprints202512.0183.v1

Article

Facile and One-Pot Photochemical Synthesis of Highly Conductive PEDOT:PSS: Towards Sustainable and Durable Supercapacitors

Yüsra Bahar Cakir [1], Nahid Aghabalapoor Keshtiban [2], Fatih Can Sarı [2], Ali Gelir [2] and Kerem Kaya [1,*]

[1] Chemistry Department, Istanbul Technical University, Maslak, Istanbul, 34469 Turkey

[2] Physics Engineering Department, Istanbul Technical University, Maslak, Istanbul, 34469 Turkey

* Correspondence: kkaya@itu.edu.tr

Abstract

The synthesis of poly(3,4-ethylenedioxythiophene):poly(styrenesulfonate) (PEDOT:PSS) a benchmark conducting polymer frequently researched for energy storage, conventionally relies on corrosive and toxic reagents leading to significant hazardous waste, conflicting with the principles of green and sustainable chemistry. This report introduces a fully photochemical, metal-free, and sustainable method that employs a single organic photoinitiator, phenacyl bromide (PAB), to achieve the *in-situ* polymerization of 3,4-ethylenedioxythiophene (EDOT) and sodium 4-styrenesulfonate (NaSS) monomers. The reaction occurs at room temperature in a benign ethanol/water solvent system. A major environmental advantage is the elimination of hazardous metal waste, replaced instead by acetophenone, a non-toxic byproduct readily removed via simple precipitation. Structural analysis confirmed the formation of the doped polymer with a PEDOT:PSS molar ratio of approximately 1:3, consistent with both Nuclear Magnetic Resonance (NMR) and X-ray photoelectron spectroscopy (XPS) bulk and surface measurements, respectively. As a proof-of-concept for its application in energy storage, the resulting PEDOT:PSS/Activated Carbon composite was fabricated into a symmetric supercapacitor device demonstrating an exceptional operational durability, retaining 97% of its initial capacitance after 2000 charge–discharge cycles. Moreover, this light-driven synthesis can enable spatiotemporal control, opening new pathways for sustainable advanced manufacturing, such as 3D printing of PEDOT:PSS, in line with SDG 9 goals.

Keywords: conductive polymers; PEDOT:PSS; photopolymerization; energy storage; supercapacitors

1. Introduction

Conducting polymers are utilized in many technologies including energy storage, optoelectronics, and sensing due to their tunable electrical conductivity and electrochemical properties.[1–7] Poly(3,4-ethylenedioxythiophene): poly(styrenesulfonate) (PEDOT: PSS) is benchmark material in this class, due for its high stability, processability in aqueous dispersions, excellent electrical and mechanical features.[8,9] Especially over the past two decades, PEDOT:PSS has been widely applied in coatings, transparent electrodes, sensors, and as an electrode material in electrochemical capacitors which are often referred to as supercapacitors (SCs).[10–12]

PEDOT:PSS is a mixed ion-electron conductor, where PEDOT chains provide electronic conductivity and PSS chains provides charge neutrality and ionic transport. This structure enables rapid redox-driven charge storage, making PEDOT:PSS ideal for high-performance SC electrodes.[13,14] Therefore, researchers have utilized its solution processability and mechanical flexibility to develop SCs in various configurations, including symmetric,[15] asymmetric,[16] microscale,[17] and hybrid designs.[18] For instance, a symmetric SC with PEDOT: Nafion achieve ~98.7% capacitance retention after 1,000 cycles.[19] Asymmetric designs, such as MnO_2/PEDOT on

 doi:10.20944/preprints202512.0183.v1

activated carbon cloth paired with carbon, expanded the voltage window, enhancing energy density without compromising power.[20] Micro-SCs printed with AC/PEDOT:PSS composites exhibit areal capacitances of ~29.5 mF cm^{-2}, nearly double that of carbon-only devices (~15.7 mF cm^{-2}), with ~85% retention after 5,000 cycles.[21] Flexible formats, such as reduced graphene oxide (rGO)–PEDOT:PSS films and carbon nanotube (CNT)-reinforced composites, offer high areal capacitance, low internal resistance, and robust cycle life.[22,23] These advancements highlight PEDOT:PSS composite as a versatile platform, tunable with carbon nanomaterials, metal oxides, or secondary dopants to optimize power, energy, flexibility, and durability.

Despite progress in the engineering PEDOT-based SCs, the synthesis of PEDOT:PSS remains a challenge for sustainable chemistry. Conventional polymerization of EDOT uses toxic and corrosive reagents like $FeCl_3$ [24] generating metal waste [25,26] or sophisticated electrochemical setups that conflict with sustainable chemistry principles.[27] Moreover, commercial PEDOT:PSS production involves separate synthesis of PEDOT and PSS, followed by mixing, making it a non-straightforward multi-step process.[28,29]

Photopolymerization offers a more sustainable alternative, leveraging light to initiate reactions without metal catalysts.[30–32] Benefits include energy efficiency, elimination of toxic and corrosive oxidants, spatiotemporal control (key for 3D printing applications),[33] and intrinsic doping.[34,35] Our group previously demonstrated photochemical oxidative polymerization of EDOT under both UV and visible light using an organic photoinitiator in ethanol,[36] light-driven copolymerization reactions of EDOT with ε–caprolactone[37] and 9-ethylcarbazole monomers[38] producing a conductive scaffold and a black-to-transmissive electrochromic copolymer, respectively. Very recently, we reported the photochemical *in situ* synthesis of PEDOT-coated polydopamine as a SC electrode material with improved ion transport and thus, better capacitive performance compared to previously obtained PEDOT-based SC electrode materials.[39]

Building on these advances, the present work introduces a straightforward one-pot photopolymerization method for the synthesis of PEDOT: PSS, by simultaneously polymerizing EDOT and NaSS (sodium 4-styrenesulfonate) monomers using phenacyl bromide (PAB) under UV-A light in a green solvent system. While hybrid systems have been reported that use conventional chemical oxidants (e.g., $FeCl_3$ for EDOT polymerization in parallel with a separate photopolymerization mechanism for a functionalized PSS scaffold[40], a fully light-driven, metal-free synthesis from simple monomers remains elusive. The primary objective of this work is to demonstrate that this sustainable synthesis route yields a high-quality material capable of delivering exceptional long-term electrochemical performance, as measured by supercapacitor cycling durability. The success of this approach is crucial for establishing green chemistry pathways for future high-performance, sustainable energy storage components.

2. Experimental Section

2.1. Materials

3,4-ethylenedioxythiophene (EDOT, 97% Sigma), sodium 4-styrenesulfonate (NaSS, ≥90% Sigma), methanol (technical grade), ethanol absolute (98%, Sigma) poly(vinylidene fluoride) (PVDF) (≥99.5 %, 600 kDa, Nanografi), 2- propanol (IPA) (Sigma Aldrich, ≥99%), *N*-methyl-2-pyrrolidone (NMP) (Sigma Aldrich, ACS reagent, ≥99.0%), polyethylene glycol (PEG) (Sigma Aldrich, average M_n 20 kDa), ethylene glycol (EG) (Sigma Aldrich, ReagentPlus, ≥99%) were used as received. 2-Bromoacetophenone (phenacyl bromide (PAB), 98% Sigma) was recrystallized from its ethanol solution. All the solutions were prepared with solvents purged with nitrogen gas, and all reactions were conducted under nitrogen atmosphere to prevent oxygen interference. For electrode fabrication, an activated carbon (AC) with relatively high surface area (on the order of 800 m^2/g) was used as received. 1 M H_2SO_4 (aq) was used as the electrolyte for the three-electrode supercapacitor tests.

 doi:10.20944/preprints202512.0183.v1

2.2. Synthesis Methods

2.2.1. Photochemical Synthesis of PSS

In a typical photopolymerization experiment, equimolar amounts of NaSS (0.48 g, 2.3 mmol) and PAB (0.47 g, 2.3 mol) were mixed using an ethanol/water mixture (4.5 mL Ethanol + 2 mL H_2O) in a Schlenk tube that was previously degassed under nitrogen atmosphere. The reaction mixture was then irradiated inside a photoreactor equipped with a magnetic stirrer, a cooling fan, and 18 fluorescent lamps (Philips TL 18 W BLB) emitting light nominally at 365 nm with a light intensity of ~100 mW/cm^2 at the reaction flask (measured using a Delta OHM Quantum radiophotometer) (Figure S1). After 72 h of irradiation, the reaction mixture was precipitated into diethyl ether then the remaining filtrates were dried under vacuum at room temperature for 48 h.

2.2.2. Photochemical In Situ Synthesis of PEDOT:PSS

In a typical photopolymerization experiment, equimolar amounts of EDOT and NaSS (EDOT (250 µL, 2.3 mmol), sodium 4-vinylbenzenesulfonate (0.48 g, 2.3 mmol)) were mixed with excess PAB (1.4 g, 7 mmol) in an ethanol/water mixture (4.5 mL ethanol + 2 mL H_2O) inside a Schlenk tube that was previously degassed under nitrogen atmosphere. The reaction mixture was then irradiated inside the same photoreactor used for PSS synthesis for 72 h. The initially colorless solution began to change color after a few minutes of UV exposure, transitioning through light blue to a dark blue coloration, indicative of PEDOT formation (Figure S2). After irradiation, the reaction mixture was a black colored dispersion containing PEDOT: PSS. Control experiments conducted in the absence of UV light (keeping the mixture in the dark under otherwise identical conditions) or in the absence of PAB resulted in no color change or precipitate formation, confirming that polymerization is indeed photo-induced by the decomposition of PAB. After 72 h of /irradiation, the product was precipitated into diethyl ether/methanol (to remove residual PAB, its side product acetophenone, sodium bromide and oligomeric products). Finally, the resulting filtrates were dried under vacuum at room temperature for 48 h.

2.3. Preparation of the PEDOT-PSS-Based SC Electrode Materials and Symmetric Device

Two separate centrifuge tubes were fixed on a stirrer. To the first tube, PVDF (5 mg, 600kDa) and NMP (0.5 mL) were added and allowed to mix, while PEDOT-PSS (250 mg, 1.35 wt%), water (16.6 mL), IPA (1.27 mL), EG (0.112 mL), and PEG (1 mg) were sequentially added to the second tube. After both mixtures had been stirred for 1 h and ultrasonicated for 1 h, they were combined and stirred for an additional 12 h to obtain a mixture suitable for the SC electrode preparation. For the SC electrode containing activated carbon (AC), 50 mg of AC (20 wt% of PEDOT: PSS) was added into the same mixture.

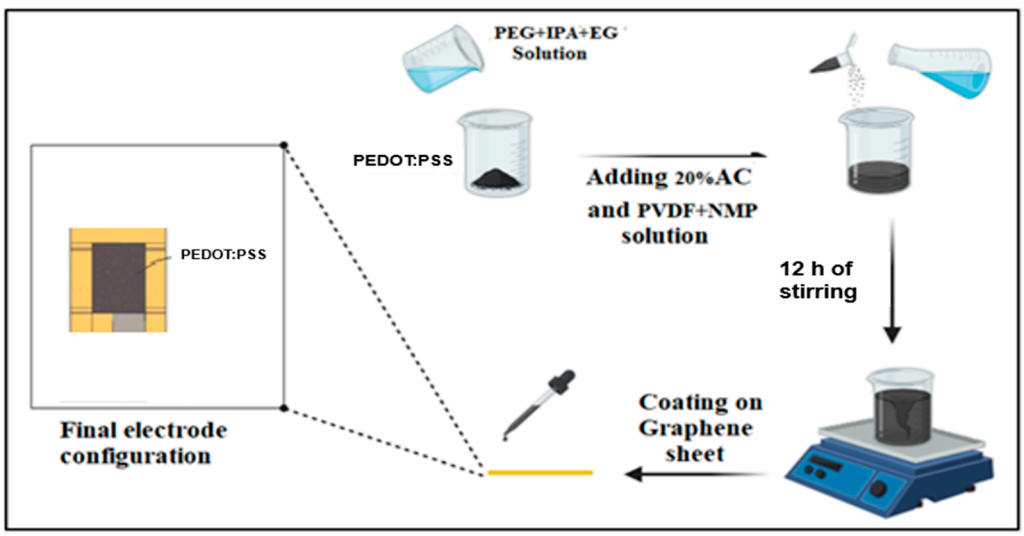

 doi:10.20944/preprints202512.0183.v1

Figure 1. Schematic illustration of the fabrication process of the PEDOT:PSS/AC (20 wt% activated carbon) sandwich electrode.

PEG was incorporated to enhance the mechanical flexibility and elasticity of the resulting film, thereby preventing cracking during the drying process and operational handling.[39] EG acted as a secondary dopant, improving the electrical conductivity of PEDOT-PSS by facilitating polymer chain rearrangement.[39] IPA was added to improve surface wettability and ensure uniform and smooth coating of the graphene substrate.[41] PVDF dissolved in NMP was introduced into the formulation to function as a binder, reinforcing the mechanical strength and adhesion of the film.[42] Activated carbon (20 wt%) was added to increase the electrochemically active surface area in the electrode.[43] The prepared slurry of PEDOT:PSS, after mixing with 20 wt% activated carbon and continuous stirring for 4 h, was subsequently deposited onto the designated current collector by a drop-casting method. The coated substrates were then dried on a hot plate at 60 °C to remove residual solvent and consolidate the electrode film.

2.4. Characterization Methods

Gel permeation chromatography measurements were performed on a TOSOH EcoSEC GPC system equipped with an auto sampler system, a temperature-controlled pump, a column oven, a refractive index (RI) detector, a purge and degasser unit and TSKgel superhZ2000, 4. 6 mm IDx 15 cm × 2 cm column. Tetrahydrofuran (THF) or dimethyl formamide (DMF) was used as an eluent at flow rate of 1.0 mL min^{-1} at 40°C and 0.5 mL min^{-1} at 60°C, respectively. While THF column system was calibrated with polystyrene (PS) standards DMF column system (with 0.1 M $NaNO_3$) was calibrated with polymethylmethacrylate (PMMA) standards having narrow molecular-weight distributions. GPC data were analyzed using Eco-SEC Analysis software.

UV–visible spectra were recorded with a Shimadzu UV-1601 double beam spectrometer equipped with a 50 W halogen lamp and a deuterium lamp which can operate between 250 nm - 1000 nm.

Fourier-transform infrared (FTIR) spectra were recorded on a Perkin–Elmer Spectrum One spectrometer using ATR technique and mercury cadmium telluride (MCT) detector. 128 scans were averaged.

^{1}H NMR and ^{13}C NMR spectra were recorded using deuterated water (D_2O) solvent at 500 MHz and 125 MHz, respectively, on an Agilent VNMRS 500 spectrometer at 25°C.

The Brunauer–Emmett–Teller (BET) measurement was conducted using Quantachrome® ASiQwin™, version 3.01 of Quantachrome Instruments. The surafce area of the activated carbon (AC) was evaluated by nitrogen adsorption–desorption isotherms at 77 K.

X-ray photoelectron spectroscopy (XPS) measurements was collected on a Thermo-Scientific K-Alpha Plus X-ray photoelectron spectrometer using Al Kα source. CasaXPS software was used to resolve and integrate the area of 2 Sp peaks.

TEM images were obtained with a JEOL JEM 1400 Plus TEM device at 80 kV operating voltage. The TEM samples were prepared with 50 µL of ethanol. 10 µL of each solution was deposited on a carbon-supported copper 300-mesh grid after 5 mins of ultrasonication and then dried at room temperature for 1 h before the analysis.

SEM images were measured using a JEOL JSM7100-F scanning electron microscope (SEM) EHT = 10 kV and a probe at 200 nA. The electromagnetic noise was minimized by covering the system with an acoustic chamber.

Water contact angle measurements were performed using the sessile drop method with a water drop volume of 10 µL on a contact angle system (Dataphysics, Contact Angle System OCA 20) at ambient temperature and 50% RH (relative humidity).

Electrical conductivities were measured at room temperature by using the standard 4-point probe technique on the electrodes prepared for the electrochemical measurements in air at room temperature and 50% RH using a HP3478A digital voltmeter, with a direct 4-wire resistance capability.

 doi:10.20944/preprints202512.0183.v1

2.5. Electrochemical Measurements

Electrochemical performance was first evaluated in a three-electrode configuration using 1 M H_2SO_4 as the electrolyte, where a platinum wire served as the counter electrode and Ag/AgCl was employed as the reference electrode. The working electrode was tested in two forms: initially as a pristine PEDOT:PSS film to assess its intrinsic electrochemical properties, and subsequently as a PEDOT:PSS composite containing 20 wt% activated carbon (AC) to evaluate the effect of the additive. In both cases, the electrodes were coated onto graphene sheets.For the two-electrode measurements, a symmetric sandwich-type device was assembled by placing two identical coated electrodes face-to-face, separated by cellulose paper impregnated with 1 M H_2SO_4, which acted as both electrolyte reservoir and separator. The electrochemical performance of this two-electrode system was then systematically evaluated.

The configuration of the symmetric device characterization is a standard two-electrode setup with no reference electrode; all electrochemical measurements thus reflect the performance of the full device, and reported specific capacitances are on a per total mass of both electrodes (device-level) basis.

$$C = \frac{I\,\Delta t}{m\,\Delta V} \tag{1}$$

where I is the discharge current *(A)*, Δt is the discharge time *(s)*, ΔV is the potential window during discharge after removing the *IR* drop *(V)*, and m is the mass of the active material *(g)*. The energy density of the device *(Wh/kg)* was calculated using:

$$E = \frac{1}{2}\Delta V^2 C \tag{2}$$

where C is the specific capacitance *(F/g)*, ΔV is the potential window *(V)*. The power density (*W/kg)* was determined:

$$P = \frac{E}{\Delta t} \tag{3}$$

where E is energy density and Δt is the discharge time (*s*). These parameters were employed to evaluate the energy-storage performance of the supercapacitor in both three-electrode and symmetric two-electrode configurations. EIS was conducted in the frequency range 100 kHz to 0.1 Hz to assess the internal resistance and ion diffusion characteristics. All measurements were done at room temperature. Prior to measurements, all the cells were cycled a few times to reach a stable state.

To distinguish between capacitive-controlled and diffusion-controlled contributions in the charge storage process, Dunn's method was employed based on cyclic voltammetry (CV) measurements at different scan rates. The current response at a given potential is expressed as:

$$i(V) = k_1 V + k_2 \sqrt{V} \tag{4}$$

where V is the scan rate (V/s), k_1 represents the capacitive contribution, and k_2 corresponds to the diffusion-controlled process. By plotting $i/\sqrt{V}$ versus $\sqrt{V}$, the constants k_1 and k_2 can be extracted, which allows quantitative separation of capacitive and diffusion-controlled charge storage at different scan rates. This method provides mechanistic insight into the charge-storage behavior and rate capability of the electrodes.

3. Results and Discussion

3.1.1. Photopolymerization of NaSS

As a control experiment, sodium 4-styrenesulfonate (NaSS) was exposed to UV-A light (~365 nm) in the presence of phenacyl bromide (PAB) initiator (with no EDOT added), resulting in successful homopolymerization of NaSS into poly (sodiumstyrene sulfonate) (PSS). As our group previously demonstrated the capability of PAB to initiate the polymerization of styrene under UV-A

 doi:10.20944/preprints202512.0183.v1

light, mechanistically, PAB undergoes Norrish Type I photolysis, generating radical species (bromine and phenacyl radicals) that add to the vinyl group of NaSS and propagate a chain-growth polymerization to form the PSS backbone.[44] Consistent with this radical-mediated process, the reaction yielded a water-soluble beige-colored PSS that was confirmed by ^{1}H NMR spectroscopy in D_2O (Figure 2a), which showed the emergence of broad aromatic proton signals in the ~6-7.5 ppm region and the disappearance of the monomer's vinylic proton peaks (~5.2–5.8 ppm), indicating consumption of double bonds belonging to NaSS monomer. UV–Vis analysis of the product further demonstrated only UV absorptions (with a characteristic benzene-ring band observed around 250 nm), and no significant visible-light absorption (Figure 2b). Furthermore, GPC analysis indicated the presence of high molecular weight PSS species (M_n = 285 kDa) with a dispersity of $Đ$= 1.66 (Figure S3). According to SEM micrograph (Figure 2c), PSS shows a highly porous and irregular surface morphology. The polymer is composed of interconnected granular and sponge-like aggregates, with numerous open voids and channel-like features. The absence of well-defined crystalline features is consistent with the amorphous nature of PSS, as previously confirmed by powder X-ray diffractograms in the literature.[45] Importantly, such a morphology could enhance ion-accessible surface area, a property relevant when PSS is used as a polyelectrolyte dopant in conductive polymer complexes such as PEDOT:PSS.

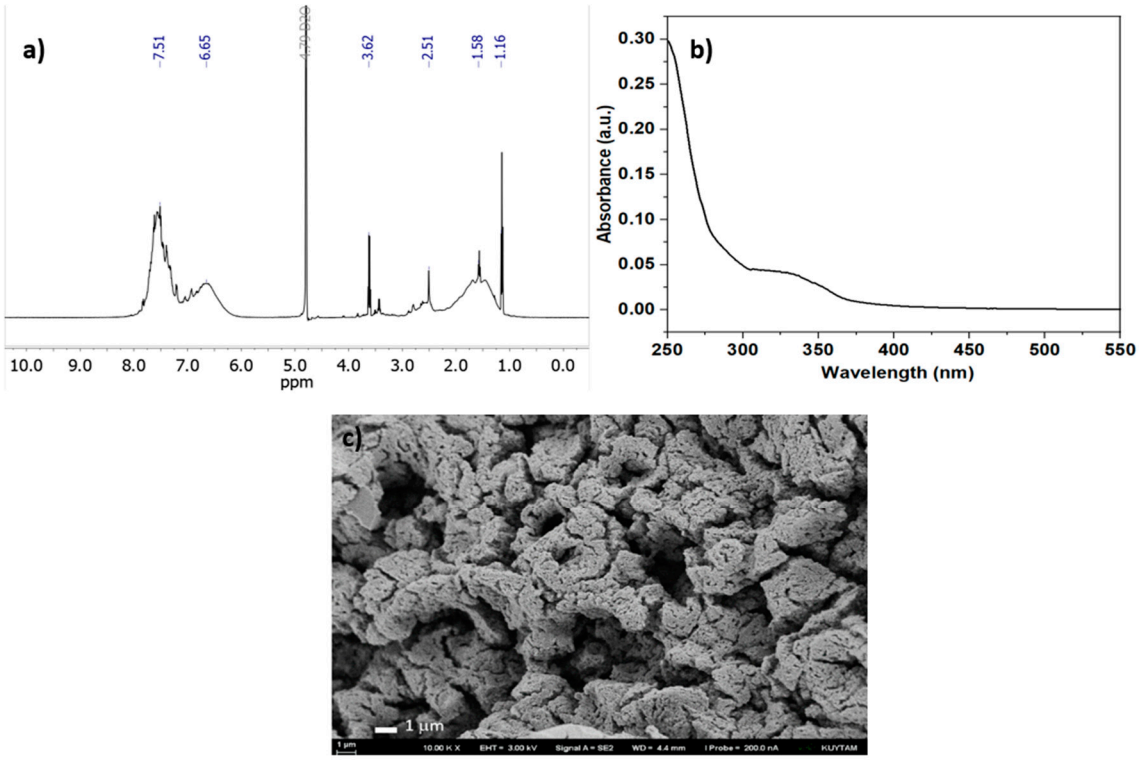

Figure 2. a) ^{1}H NMR spectrum of the photochemically obtained PSS homopolymer measured in deuterium oxide. b) UV-Vis spectrum of the PSS measured in water c) SEM micrograph of PSS displaying sponge-like aggregates with porous features.

3.1.1. Light-Induced One-Pot Synthesis and Characterization of PEDOT:PSS

Homopolymerization of NaSS experiment confirms that NaSS is indeed photochemically reactive under the same UV-A/PAB conditions, supporting the one-pot PEDOT:PSS synthesis pathway as the homopolymerization of EDOT under the same conditions was previously demonstrated by our group.[36] In the main reaction, NaSS can undergo *in situ* radical polymerization to form PSS concurrently alongside the photooxidative polymerization of EDOT initiated by bromine radicals, thereby providing a readily-formed polyanionic PSS matrix that both dopes and stabilizes the growing PEDOT chains.

 doi:10.20944/preprints202512.0183.v1

Light-induced polymerization of EDOT in the presence of NaSS and PAB was successful in yielding PEDOT:PSS without any additional chemical oxidant. The reaction mixture's rapid color change from colorless to first dark blue and then to dark green and finally to black under UV-A irradiation confirmed the quick formation of conjugated polymer chains. In contrast, no polymer was formed when the mixture was kept in the dark, underscoring that photoactivation of PAB is essential for the polymerization.

Based on our previous findings of laser-flash photolysis,[39] we propose that the photogenerated bromine radicals abstract an electron to produce radical cations on EDOT, which then couple to form PEDOT chains in step-growth fashion. Simultaneously, NaSS monomers can polymerize through the initiation of both phenacyl and bromine radicals, forming PSS chains or attach as side-groups, effectively and *in situ* doping the PEDOT with sulfonate anions. The overall result is a doped PEDOT:PSS network formed in one pot (Scheme 1).

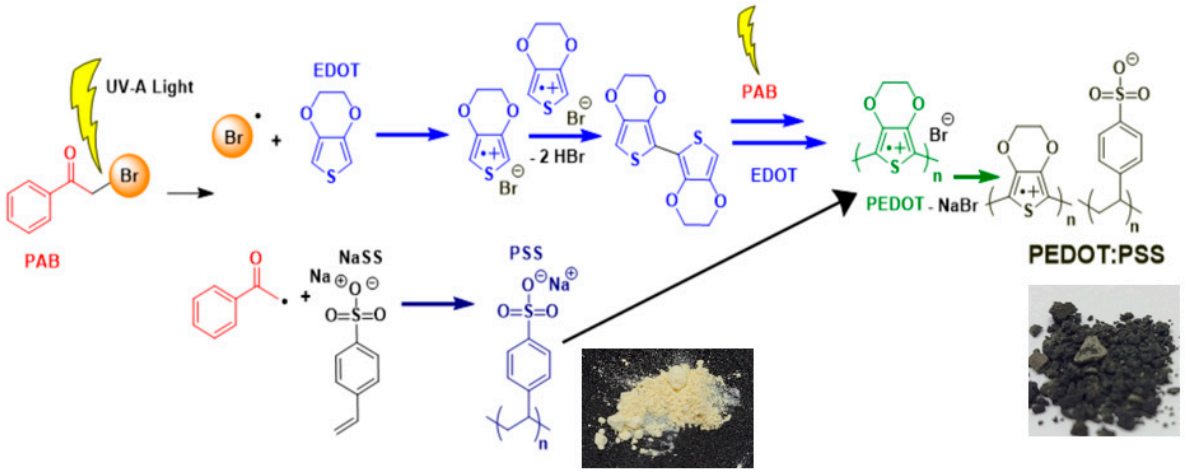

Scheme 1. Light-Induced Synthesis of PEDOT:PSS via PAB-Mediated One-Pot Photopolymerization of EDOT and NaSS.

This methodology offers several noteworthy advantages such as (i) Mild Conditions: The polymerization proceeds at room temperature under light, avoiding the heating often required in chemical oxidations. (ii) Green Solvent: Ethanol/Water mixture is used as the medium, which is an environmentally benign solvent system. (iii) No Hazardous Oxidants: Traditional oxidants like $FeCl_3$ or persulfates are replaced by an organic photoinitiator, simplifying purification since the major byproducts is non-toxic and highly soluble acetophenone that can easily be removed during precipitation. (iv) *In Situ* Doping: Because the PSS is synthesized during polymerization, the resulting PEDOT is obtained directly in its doped state (with PSS^- counter anions), eliminating the need for a separate synthesis/doping step to achieve conductivity. Overall, all these features make this photopolymerization method a compelling new approach for PEDOT:PSS.

Table 1. Sustainability-focused comparison of PEDOT:PSS synthesis methods.

Method	Oxidant / Initiator	Solvent System	Byproducts & Waste	Process Features & Sustainability Impact
This Work (Photochemical)	Organic Photoinitiator (Phenacyl Bromide)	Benign (Ethanol/Water)	Acetophenone (Non-toxic, readily removed)	**One-Pot, in situ Doping:** Eliminates need for separate blending. Metal-free process avoids hazardous waste. Enables spatiotemporal control for 3D printing.
Conventional Chemical	Corrosive Oxidants (e.g., $FeCl_3$, persulfates)	Aqueous / Acidic	Generates metal waste/corrosive byproducts.	**Multi-Step:** Often requires separate synthesis and blending of PEDOT and PSS. Product requires extensive purification to remove metal contaminants.

 doi:10.20944/preprints202512.0183.v1

Electrochemical	Applied Potential (Electricity)	Electrolyte Solution	No major chemical waste	**Setup-Intensive:** Requires sophisticated electrochemical setups and a conductive substrate. Not scalable for bulk ink/powder synthesis.

Excess of the photoinitiator (PAB) (compared to EDOT and NaSS) was necessary for a significant NaSS conversion since equimolar amounts of PAB resulted in unreacted monomer (NaSS) present in PEDOT:PSS that was confirmed by ^{1}H NMR spectroscopy (Figure S4). The photochemically obtained PEDOT:PSS having a gravimetric monomer conversion of 42%, is a dark-blue to black colored, powdery solid that disperses well in water due to the PSS content (Figure S5).

The GPC traces indicated a number-average molecular weight M_n = 2300 g/mol and a relatively narrow molecular weight distribution with a dispersity index of $Đ$= 1.4 (Figure S6), signifying the detection of PEDOT species more than PSS. While GPC revealed a high apparent molecular weight for the homopolymer PSS (Figure S3), whereas the PEDOT:PSS complex displayed a substantially lower molecular weight. We attribute this difference to both chemistry and GPC hydrodynamics. First, radical homopolymerization of NaSS under UV-A/PAB yields high-molecular-weight PSS, while photochemical oxidative coupling of EDOT intrinsically produces short PEDOT chains (limited by chain-transfer/termination), so the PEDOT fraction is genuinely low-M_w. Second, upon complexation the PEDOT:PSS forms compact ionic nanocomplexes; relative to free PSS of the same mass, exhibiting smaller hydrodynamic volume and stronger column interactions, causing later elution and underestimation of M_w in PMMA-calibrated GPC.

^{1}H NMR spectrum of the photochemically obtained PEDOT:PSS (Figure 3a) revealed broadening of peaks corresponding to the ethylenedioxy protons (-O-CH$_2$-) of the PEDOT repeating unit at ~4.2-4.4 ppm, as well as aromatic signals in the 7.5–8.3 ppm range attributed to the hydrogens of the PSS dopant. The absence of peaks for the monomers (EDOT's vinyl protons around 6.3 ppm and NaSS styrenic protons around 5.5 ppm) indicates successful polymerization. Semi-quantitative integration of the PSS aromatic and PEDOT ethylenedioxy regions (4 H vs 4 H) yields a PEDOT:PSS molar ratio on the order of 1:3, similar to commercially available charge-balanced PEDOT:PSS solution sold under the name Clevios™ P VP AI 4083.[46] ^{13}C NMR signals are often undetectable in PEDOT:PSS solution, making solid-state CP/MAS the standard method for structural characterization.[47] In this context, the solution-state ^{13}C NMR spectrum obtained in our study provides rare complementary evidence of both PEDOT and PSS backbones, even though the resonances are broad, consistent with the conductive, partially doped state of the polymer. ^{13}C NMR spectrum of the photopolymerized PEDOT:PSS (Figure S7) displayed broad resonances centered at δ ≈ 128 ppm, corresponding to the aromatic carbons of the PSS matrix, along with distinct signals at δ ≈ 65–70 ppm assigned to the ethylenedioxy groups (–O–CH$_2$–) of PEDOT. Importantly, no vinyl carbon signals were observed in the δ 120–140 ppm region, confirming complete consumption of EDOT and NaSS monomers. The broad nature of the peaks is characteristic of conducting polymers in the doped state, where delocalized polarons shorten relaxation times.[48] These observations verify the successful *in situ* photopolymerization of EDOT and NaSS.

X-ray photoelectron spectroscopy (XPS) was employed (Figure S8) to investigate the surface chemistry and elemental composition of the PEDOT:PSS powder and compare the PEDOT:PSS ratio with the one calculated from NMR spectrum. The XPS survey scan confirmed the presence of the three primary elements expected for a PEDOT:PSS blend: carbon (C 1s), oxygen (O 1s), and sulfur (S 2p). The quantitative analysis of the survey scan, showed a high carbon content (71.49%) and a significant presence of oxygen (19.16%) and sulfur (5.67%). The analysis also detected minor amounts of sodium (Na 1s) (3.04%) and bromine (Br 3p) (0.63%). While Na is present in most of the PEDOT:PSS as residual,[49] bromine likely remains as a residual impurity from the oxidative polymerization of EDOT, where bromide salts are present as counter-ions to positively charged PEDOT species. To determine the molar ratio of PEDOT to PSS, a high-resolution scan of the S 2p core level was conducted. The spectrum was successfully deconvoluted into two distinct doublets, corresponding to two different chemical environments for sulfur (Figure S9). A doublet with the S 2p$_{3/2}$ peak centered

 doi:10.20944/preprints202512.0183.v1

at a lower binding energy (~162 eV) was assigned to the sulfur atoms in the thiophene ring of the PEDOT component. This low binding energy is characteristic of non-oxidized, aromatic sulfur [50] A second doublet with the S $2p_{3/2}$ peak at a higher binding energy (~166 eV) was assigned to the highly oxidized sulfur atoms in the sulfonate group ($-SO_3^-$) of the PSS component. The integral areas of these two doublets were used to quantify the relative abundance of each polymer on the powder's surface. The analysis revealed that the PEDOT peak contributed 23.4% and the PSS peak contributed 76.6% to the total S 2p signal area, corresponding to a surface molar ratio of PEDOT:PSS = 1:3.2. This result is in good agreement with the ratio determined by NMR analysis (1:3), though the slight difference might be due to the surface-sensitive nature of XPS compared to the bulk analysis of NMR.

UV-Vis absorption spectrum measured for PEDOT:PSS in water displayed a peak between 600-900 nm characteristic of doped PEDOT (Figure 3b). This broad absorption extending from the visible into the near-infrared region is typical for highly conjugated polymer chains in a doped (conductive) state. The similarity of this spectrum to commercial PEDOT:PSS dispersions further confirms the successful *in situ* photopolymerization of EDOT and NaSS.[51]

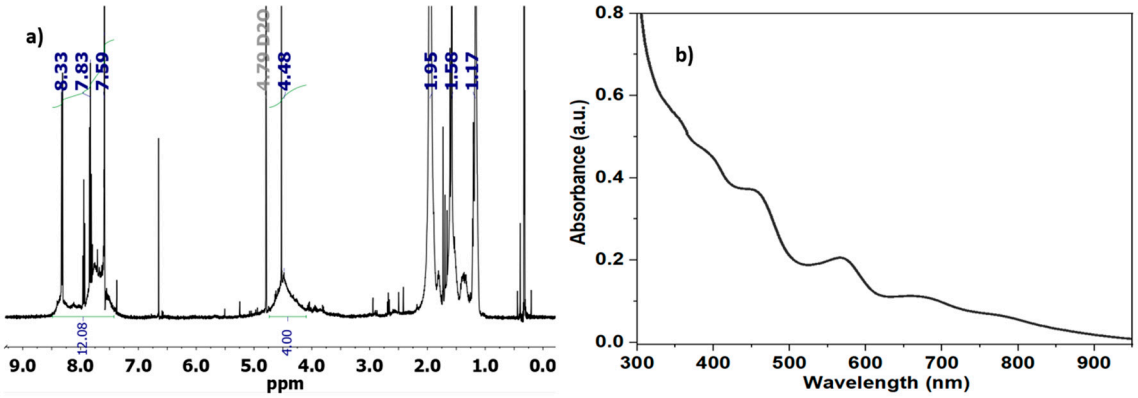

Figure 3. a) ^{1}H NMR spectrum of the photochemically synthesized PEDOT:PSS measured in deuterium oxide displaying broadening of the peaks belonging to both PEDOT and PSS fragments and b) UV-Vis spectrum of the water solution of the reported PEDOT:PSS showing a broad absorption extending to NIR region.

In the IR data of the photochemically obtained PEDOT:PSS (Figure S10), the combination of strong SO_3^- bands (PSS) near 1180 cm^{-1} with the C–O–C (ethylenedioxy) near 1200 cm^{-1} and thiophene signature peaks at 700-900 cm^{-1} region verifies the formation of the PEDOT:PSS.[52] The broadened, intense absorption in the 1200–1500 cm^{-1} region is consistent with doped PEDOT (polaronic character) aligning with the UV–Vis tail into the visible–NIR. Overall, the IR data corroborate successful one-pot photopolymerization of EDOT and NaSS.

The wettability of the electrode surfaces was assessed by water contact angle (WCA) measurements (Figure S11). The pristine PEDOT:PSS electrode exhibited a low contact angle of 21°, indicative of its high hydrophilicity, which can be attributed to the presence of sulfonate groups in PSS that promote strong interactions with water. Upon incorporation of 20 wt% activated carbon (PEDOT:PSS/AC composite), the contact angle increased slightly to 26°, reflecting a modest reduction in hydrophilicity due to the relatively hydrophobic nature of carbon surfaces. Nevertheless, both values fall within the hydrophilic regime ensuring effective electrolyte wetting and facilitating ion transport at the electrode/electrolyte interface.

Transmission electron microscopy (TEM) reveals the nanoscale morphology of the photochemically synthesized PEDOT:PSS (Figure 4a,b). The image displays a heterogeneous distribution of PEDOT-rich domains embedded within the PSS matrix. The darker, higher-contrast regions correspond to the π-conjugated PEDOT backbone, whereas the lighter, diffuse areas represent the amorphous and insulating PSS component. The observed morphology suggests the formation of interconnected PEDOT clusters with sizes ranging between approximately 50–200 nm, which are uniformly distributed throughout the sample. Such a nanophase-separated structure is

 doi:10.20944/preprints202512.0183.v1

characteristic of PEDOT:PSS[53] and plays a crucial role in its electrical properties: the percolated PEDOT domains facilitate charge transport, while PSS ensures colloidal stability and film formation. This nanoscale morphology is advantageous for applications in energy storage, as it maximizes interfacial contact, improves charge mobility, and enhances electrochemical accessibility.[54] The absence of large aggregates or phase segregation further supports that photopolymerization yields a homogeneous polymer network, which is expected to contribute to the improved electrochemical stability.

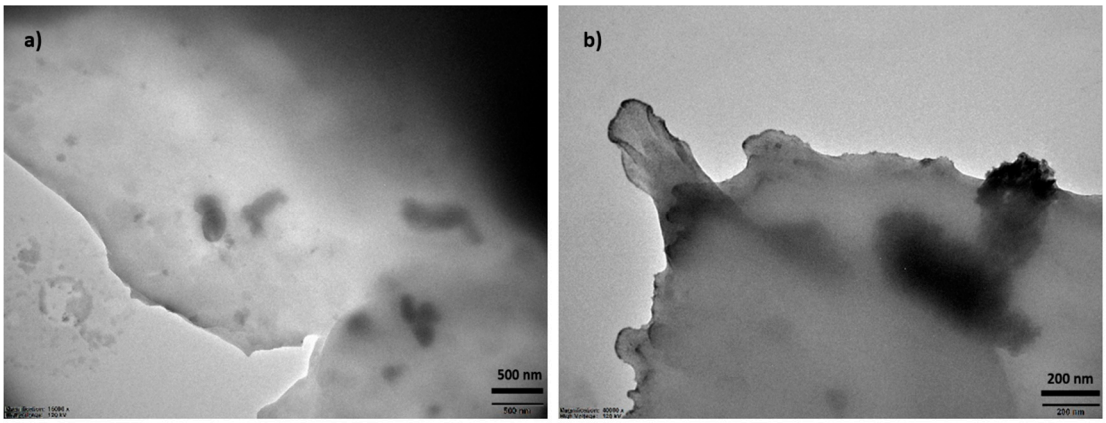

Figure 4. TEM micrographs of photopolymerized PEDOT:PSS at different magnifications: (a) lower-magnification view showing the amorphous polymeric matrix with diffuse contrast and granular features, and (b) higher-magnification image highlighting irregular, non-crystalline domains and local density variations typical of the phase-separated PEDOT:PSS structure**.**

We added 20 wt% activated carbon to the photochemically prepared PEDOT:PSS to exploit the complementary charge-storage mechanisms: the carbon contributes large double-layer capacitance from its high surface area, whereas PEDOT:PSS supplies electronic conductivity and pseudocapacitance. This hybridization is well-known to balance surface-driven and redox-driven storages, yielding higher specific capacitance and better cycling stability than pristine PEDOT:PSS in electrical storage applications.[13] Surface area of AC used in this experiment was calculated using BET (Brunauer-Emmett-Teller) testing using the gas sorption data acquisition and reduction and calculated as 794 g/m^2 confirming the high porosity and suitability of AC as an electrochemical double-layer charge storage component (Figure S12). The morphology of the photochemically obtained PEDOT:PSS and its combination with 20 wt% activated carbon (AC) (PEDOT: PSS/AC) was examined by scanning electron microscopy (SEM) (Figure 5a,b).

The SEM micrograph of pristine photopolymerized PEDOT:PSS (Figure 5a) reveals a relatively smooth and compact granular surface, with polymer domains forming a continuous film but displaying limited porosity. Such morphology is characteristic of pristine PEDOT:PSS, where PEDOT-rich grains are embedded within a PSS-rich matrix, yielding a dense structure with modest surface area.[55] In contrast, the PEDOT:PSS composite containing 20 wt% activated carbon (PEDOT:PSS/AC) exhibits a distinctly rougher and more heterogeneous texture, with numerous voids, and particle-like features visible across the surface (Figure 5b). The AC particles are well integrated within the polymer matrix, creating an interconnected porous network. This microstructure is expected to increase electrolyte accessibility and ion diffusion pathways, while PEDOT:PSS acts as a conductive binder that electrically bridges the carbon particles. Overall, SEM analysis confirms that incorporation of AC transforms the morphology from a compact polymer film into a highly porous, composite network, a change that should theoretically result in improved electrochemical performance.

 doi:10.20944/preprints202512.0183.v1

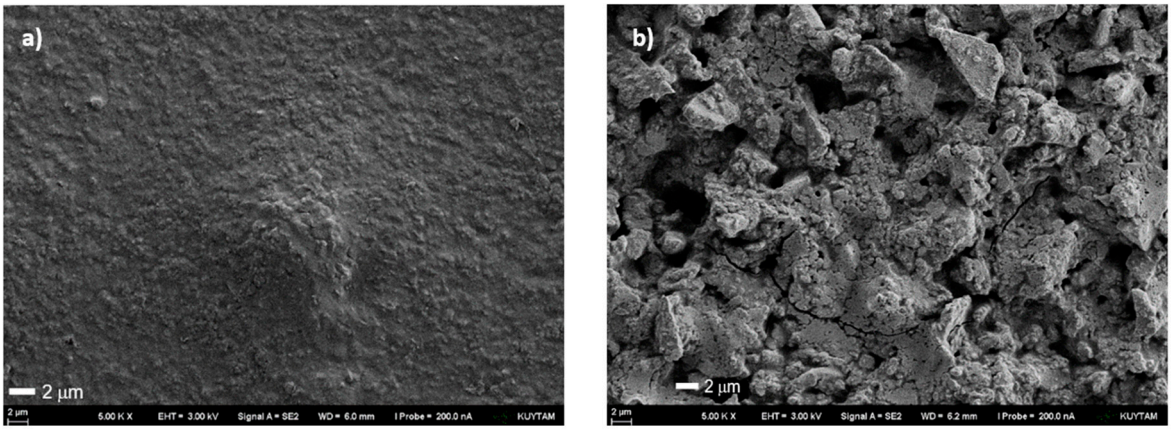

Figure 5. SEM micrographs of (a) pristine photopolymerized PEDOT:PSS, showing a relatively dense and featureless surface, and (b) PEDOT:PSS composite with 20 wt% activated carbon, exhibiting a rough, porous morphology with interconnected particulate domains favoring electrolyte penetration and ion transport in SC applications.

Electrical conductivity measurements on pressed pellets of the doped polymer revealed a remarkable electrical conductivity of 323.7 S/cm for the PEG–IPA–EG-treated, photochemically synthesized PEDOT:PSS. This improvement arises from the synergistic influence of PSS, the mixed solvent system (PEG, EG and IPA) and the advantages of photopolymerization under mild conditions. In the PEDOT:PSS composite, PSS acts as both a polyanionic dopant and a structural template, stabilizing oxidized PEDOT chains and facilitating extended π-conjugation. The PEG–IPA–EG post-treatment further reorganizes the microstructure by partially removing or redistributing the insulating PSS phase, enhancing phase separation and promoting π–π stacking among PEDOT-rich domains. Additionally, PEG assists in maintaining film flexibility and suppressing crack formation, while EG and IPA improve chain alignment and carrier mobility. Together with the defect-minimizing nature of photopolymerization, these effects yield a highly interconnected conductive network, explaining the over two orders of magnitude increase in conductivity compared to pristine PEDOT. Notably, when 20 wt% activated carbon (AC) was incorporated, the conductivity dramatically increased to 2623 S/cm, owing to the formation of enhanced interfacial charge transfer between PEDOT chains and the graphitic AC network.

3.2.1. Electrochemical Behavior of PEDOT:PSS and PEDOT:PSS/AC Electrodes

Prior to the incorporation of activated carbon (AC), the pristine PEDOT:PSS-based solution comprising PEG, EG, IPA, and PVDF/NMP was subjected to electrochemical analysis to establish a baseline performance profile. This preliminary evaluation was critical to understand the intrinsic electrochemical behavior of the binder–polymer matrix in the absence of electrochemically active fillers. Establishing this reference performance allowed for a more accurate assessment of the functional role and performance enhancement contributed by each additive.

Initial electrochemical measurements were conducted using a three-electrode configuration connected to a potentiostat system. As a first step, pristine PEDOT:PSS was tested alone to establish its baseline electrochemical response. Figure 6a presents the cyclic voltammetry (CV) curves of the pristine electrode material without activated carbon, recorded at scan rates ranging from 25 to 200 mV/s. The CV profiles have shapes that deviate from ideal capacitive behavior, indicating a combination of electric double-layer capacitance and pseudocapacitive contributions from the PEDOT:PSS matrix. As the scan rate increases, the current response also increases proportionally, which is a typical signature of good electrochemical reversibility and surface-limited charge storage.

Nevertheless, the anodic current response is more pronounced compared to the cathodic branch. This asymmetry can be attributed to the p-type nature of PEDOT, where oxidation (doping) processes

 doi:10.20944/preprints202512.0183.v1

in the positive potential region are more efficient than reduction (dedoping) processes in the negative range. Additionally, the PSS matrix restricts ion transport during dedoping, further lowering the cathodic response. As a result, the charge storage is mainly dominated by the anodic side. The relatively narrow enclosed area and low current densities, particularly at low scan rates (e.g., 25 mV/s), demonstrate that the energy storage capability of pristine PEDOT:PSS is limited. This highlights the necessity of incorporating high-surface-area materials such as activated carbon to enhance the double-layer charge storage and improve the overall specific capacitance.

Figure 6b depicts the $\log(i)$ versus $\log(v)$ plot obtained from the cyclic voltammetry data of the pristine PEDOT:PSS electrode. The linear fitting of the data yields a slope of approximately 0.4. In electrochemical systems, this parameter provides insight into the dominant charge storage mechanism: slope close to 0.5 indicates diffusion-controlled behavior, whereas a value near 1 suggests a surface-confined (capacitive) process. The observed slope of 0.40 thus confirms that the electrochemical response of PEDOT:PSS is primarily governed by ion diffusion within the electrode bulk rather than by purely capacitive surface reactions. The PEDOT:PSS electrode modified with 20 wt% activated carbon (AC) exhibited a significant enhancement in electrochemical performance, as shown in the Figure 6c–f by the CV, GCD, and kinetic analysis results.

CV curves in Figure 6c shows that the incorporation of AC led to a more rectangular and symmetric shape across various scan rates, indicating an increased capacitive character and faster charge propagation at the electrode–electrolyte interface. The galvanostatic charge–discharge (GCD) measurements confirmed this improvement as seen in Figure 6d, revealing a specific capacitance of 25 F/g, which is higher than that of pristine PEDOT:PSS.

Figure 6e illustrates the $\log(i)$ versus $\log(v)$ plot for the composite showed a slope of approximately 0.50, compared to 0.40 for the unmodified electrode. This shift in slope suggests a transition from a predominantly diffusion-controlled process toward a more balanced or mixed mechanism, with greater contribution from surface-controlled (capacitive) charge storage. The increased slope is attributed to the porous structure and high surface area of AC, which facilitate better electrolyte accessibility and more efficient ion transport, thereby improving the overall kinetics of the system.

The capacitive contribution of the PEDOT: PSS/AC (20%) electrode was further quantified as a function of scan rate, and the results are illustrated in the Figure 6f. At a low scan rate of 25 mV/s, the capacitive contribution was approximately 20%, indicating that the charge storage process at this rate is predominantly diffusion-controlled. However, as the scan rate increased, the capacitive behavior became more pronounced, reaching nearly 80% at 200 mV/s. This trend highlights a fundamental characteristic of hybrid electrode materials: at low scan rates, ions have sufficient time to diffuse into the bulk of the electrode, activating deeper redox sites; whereas at high scan rates, only surface-accessible sites participate, favoring capacitive (surface-limited) charge storage. The increased capacitive dominance at higher scan rates in the composite electrode confirms the effectiveness of activated carbon in enhancing the surface kinetics and fast electrochemical response of the system. Such behavior is desirable for high-power applications where rapid charge/discharge capability is essential.

 doi:10.20944/preprints202512.0183.v1

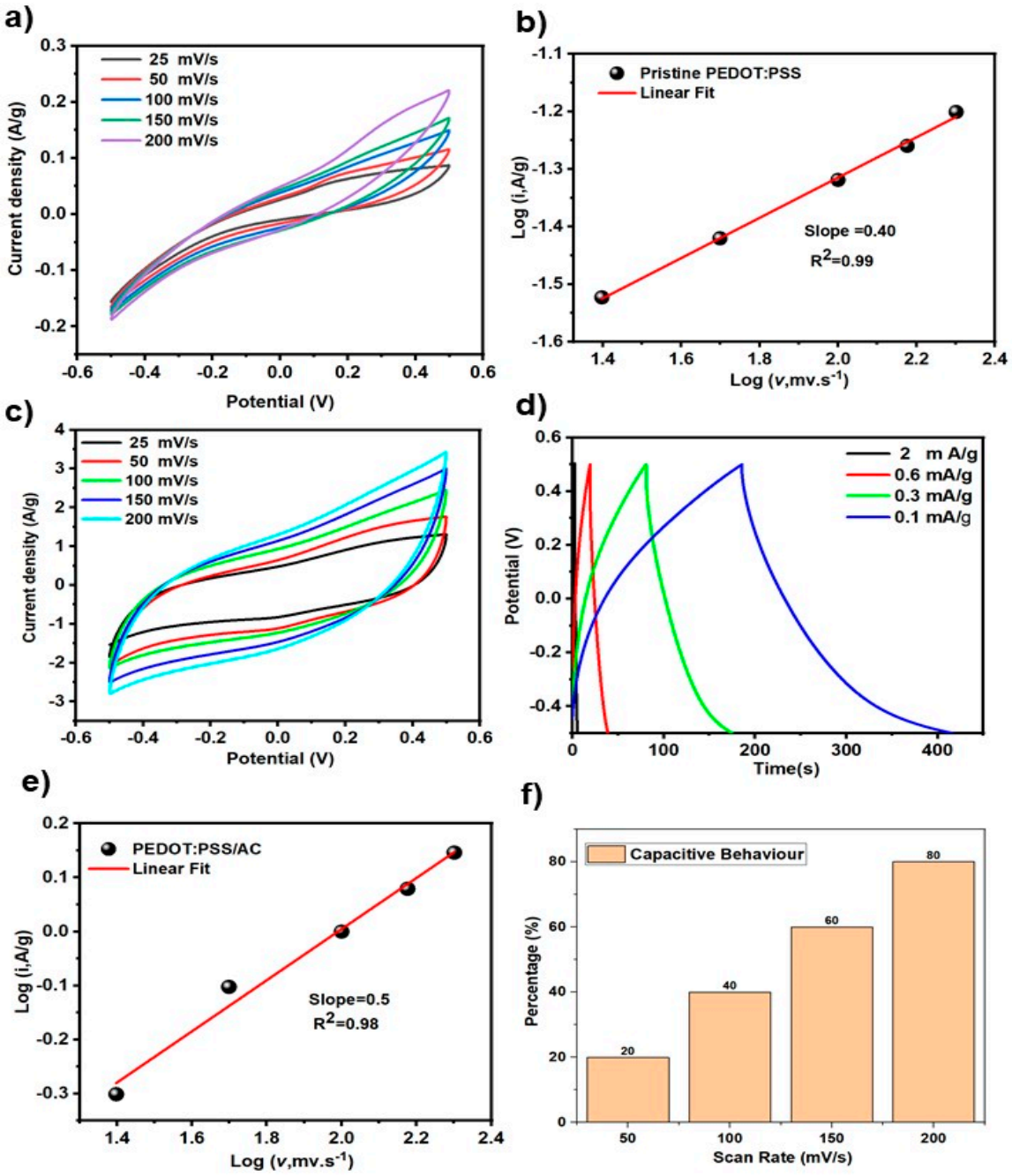

Figure 6. Electrochemical characterization of PEDOT:PSS and PEDOT:PSS/AC electrodes. (a) CV curves of pristine PEDOT:PSS at various scan rates (25–200 mV/s). (b) $\log(i) - \log(v)$ plot of PEDOT:PSS; slope 0.40 indicating diffusion-controlled behavior. (c) CV curves of PEDOT:PSS/AC showing enhanced capacitive shape. (d) GCD curves of PEDOT:PSS/AC at different current densities. (e) log(i)–log(v) plot of PEDOT:PSS/AC; slope 0.50 suggesting mixed capacitive–diffusive behavior. (f) Dunn bar graph which shows capacitive contribution at different scan rates.

In order to systematically evaluate the electrochemical performance of PEDOT:PSS/AC, a two-cell system was fabricated. The active material was prepared strictly following the procedure outlined in Figure 1, ensuring consistency in the fabrication process, and subsequently subjected to electrochemical characterization. The electrochemical tests were conducted using a cellulose-based electrolyte, which had been impregnated with 1M H_2SO_4, and the assembled cells were subsequently subjected to detailed electrochemical characterization.

The CV curves of symmetric devices constructed by PEDOT:PSS/AC electrodes, acquired at various scan rates between 25 and 200 mV/s within a potential range of -0.5 to 0.5 V, are shown in

 doi:10.20944/preprints202512.0183.v1

Figure 7a. Ideal capacitive behavior and effective charge storage are indicated by the curves which are approximately rectangular shape. As the scan rate increases, the enclosed region of the CV curves expands and the current response increases, indicating an increase in the capacitive contribution. Higher scan rates (e.g., 200 mV/s) show a little distortion from the rectangular shape, however this departure is primarily due to internal resistance and ion diffusion restrictions. Overall, the findings demonstrate that throughout a broad range of scan rates, the PEDOT:PSS/AC electrode retains its quick charge-discharge capability and stable capacitive properties.

Figure 7b shows the galvanostatic charge–discharge (GCD) profiles of device measured at different current densities (10–160 mA/g) within the potential window of –0.5 to 0.5 V. The curves exhibit a nearly symmetric triangular shape, indicating a typical capacitive behavior and efficient charge–discharge reversibility. Based on the discharge profiles, a specific capacitance of ~8 F/g was calculated at a low current density of 10 mA/g. Furthermore, the almost identical charging and discharging times reflect a high Coulombic efficiency, confirming the promising electrochemical reversibility of the electrode. The absence of an evident IR drop further demonstrates the good conductivity and low internal resistance of the composite electrode.

Figure 7c depicts the Nyquist plot of the device measured in the frequency range from 100 kHz to 0.01 Hz (inset: enlarged high-frequency region). The intercept at the real axis corresponds to the solution resistance (R_s), which is found to be relatively small, indicating good ionic conductivity of the cellulose/H_2SO_4 electrolyte. The absence of a pronounced semicircle in the high-frequency region suggests a low charge-transfer resistance (R_{ct}), further confirming efficient electron/ion transport at the electrode–electrolyte interface. At low frequencies, the plot exhibits an almost vertical line, which is characteristic of ideal capacitive behavior and efficient ion diffusion. These EIS results highlight the favorable electrochemical kinetics and low internal resistance of the PEDOT:PSS/AC composite electrodes in the device.

The log(i)–log(v) relationship for the symmetric device derived from CV measurements at various scan speeds is displayed in Figure 7d. The linear fit has an outstanding correlation coefficient ($R^2 = 0.99$) and a slope (b-value) of 0.60. Given that a surface-controlled capacitive process is indicated by a b-value of 1.0 and a diffusion-controlled process by a b-value of 0.5, the obtained slope of 0.6 implies that the charge storage in the sandwich device results from a mixed mechanism. Specifically, capacitive surface redox contributions and diffusion-limited ion intercalation coexist, with capacitive effects being marginally more significant. The desired characteristics of pseudocapacitive electrodes for high-performance supercapacitors are in line with this hybrid behavior.

Figure 7e illustrates the capacitive contribution ratio of the PEDOT:PSS/AC electrode at different scan rates, calculated at a potential of 0.15 V. The capacitive contribution increases progressively from 33% at 10 mV/s to 63% at 200 mV/s. This trend indicates that at higher scan rates, the charge storage is increasingly dominated by capacitive processes rather than diffusion-controlled contributions. Such behavior demonstrates the excellent rate capability of the electrode, as it can sustain fast charge–discharge processes with minimal diffusion limitations.

Figure 7f presents the Ragone plot of the PEDOT:PSS/AC electrode in comparison with other energy storage and conversion systems. The results indicate that the device exhibits an intermediate performance between conventional capacitors and batteries, delivering a promising balance of high-power density and moderate energy density, which is characteristic of pseudocapacitive materials. Furthermore, the long-term cycling stability shown in Figure 7g demonstrates that the electrode retains ~97% of its initial capacitance after 2000 continuous charge–discharge cycles. This excellent retention confirms the durability and structural stability of the composite, highlighting its potential for practical supercapacitor applications.

 doi:10.20944/preprints202512.0183.v1

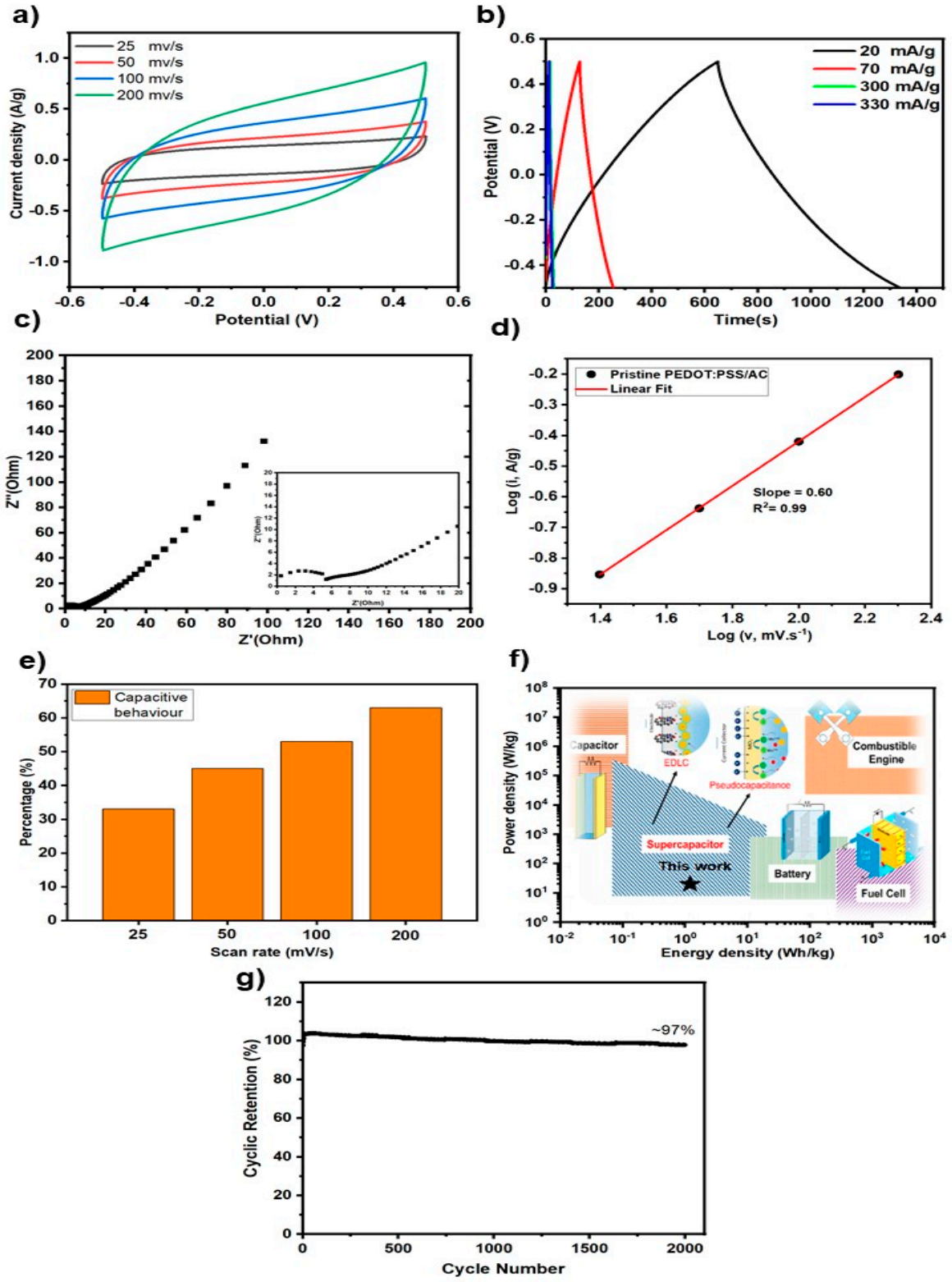

Figure 7. Electrochemical performance of PEDOT:PSS/AC (20 wt% activated carbon) sandwich electrode: (a) CV curves at different scan rates, (b) GCD profiles at various current densities, (c) Nyquist plot (EIS), (d) b-value analysis, (e) capacitance retention at different scan rates, (f) Ragone plot, and (g) cycling stability over 2000 cycles.

4. Conclusions

This work demonstrates the development of a highly sustainable, metal-free, one-pot photochemical method for the synthesis of PEDOT:PSS, a commercially available conductive polymer used for advanced energy storage. The methodology successfully eliminates the need for corrosive and toxic chemicals replacing them with an organic photoinitiator (PAB) in a benign

 doi:10.20944/preprints202512.0183.v1

ethanol/water medium. The synthesis yielded a high-quality, highly conductive polymer with a PEDOT:PSS molar ratio of ~1:3. Crucially, post-treatment resulted in an intrinsic conductivity of 323 S/cm which was further increased to 2623 S/cm when mixed with 20 wt% activated carbon. This high conductivity, combined with an optimized porous morphology, enabled efficient charge transport, as confirmed by the favorable mixed-kinetic behavior (b-value of 0.60) and low resistance observed in the symmetric device. The most significant finding is the exceptional durability of the material in a functional supercapacitor device, achieving 97% capacitance retention after 2000 charge-discharge cycles. This operational stability serves as a clear evidence that the light-induced and metal-free synthesis produces an inherently long-lasting electrode material, directly addressing the global demand for durable components that reduce toxic wastes. This work establishes a new, green pathway for the industrial production of conductive polymers, directly supporting SDG 12 (Responsible Consumption and Production) by designing out hazardous metal waste. Furthermore, the inherent spatiotemporal control offered by photopolymerization can open a new path for the advanced manufacturing techniques, such as 3D printing of PEDOT:PSS, aligning this research with SDG 9 (Industry, Innovation, and Infrastructure). Future efforts will focus on leveraging this light-driven control to realize complex micro-structured electrode patterns, paving the way for scalable, sustainable, and highly efficient next-generation energy storage devices.

Supplementary Materials: The following supporting information can be downloaded at the website of this paper posted on Preprints.org.

Acknowledgements: The authors acknowledge the support from Council of Higher Education (YÖK) Project: TGA-2025-46484 and thank Zafer Eroglu for his help on the measurements of electron microscopy.

References

1. Bryan AM, Santino LM, Lu Y, Acharya S, D'Arcy JM. Conducting Polymers for Pseudocapacitive Energy Storage. Chemistry of Materials. 2016;28(17):5989-98.
2. Masood M, Hussain S, Sohail M, Rehman A, Uzzaman MA, Alnaser IA, et al. Recent Progress, Challenges, and Opportunities of Conducting Polymers for Energy Storage Applications. ChemistrySelect. 2024;9(23):e202302876.
3. R. Murad A, Iraqi A, Aziz SB, N. Abdullah S, Brza MA. Conducting Polymers for Optoelectronic Devices and Organic Solar Cells: A Review. Polymers. 2020;12(11):2627.
4. Yoon H. Current Trends in Sensors Based on Conducting Polymer Nanomaterials. Nanomaterials (Basel). 2013;3(3):524-49.
5. Yan L, Gao X, Thomas JP, Ngai J, Altounian H, Leung KT, et al. Ionically cross-linked PEDOT:PSS as a multi-functional conductive binder for high-performance lithium–sulfur batteries. Sustainable Energy & Fuels. 2018;2(7):1574-81.
6. Zhu S, Tang M, Wu Y, Chen Y, Jiang C, Xia C, et al. Free-standing protective films for enhancing the cyclability of organic batteries. Sustainable Energy & Fuels. 2019;3(1):142-7.
7. Cha H-C, Huang S-H, Li C-F, Tsai F-Y, Su W-F, Huang Y-C. Advances and strategies in scalable coating techniques for flexible perovskite solar cells. Sustainable Energy & Fuels. 2025;9(22):5962-6006.
8. Fan X, Nie W, Tsai H, Wang N, Huang H, Cheng Y, et al. PEDOT:PSS for Flexible and Stretchable Electronics: Modifications, Strategies, and Applications. Advanced Science. 2019;6(19):1900813.
9. Alhashmi Alamer F, Althagafy K, Alsalmi O, Aldeih A, Alotaiby H, Althebaiti M, et al. Review on PEDOT:PSS-Based Conductive Fabric. ACS Omega. 2022;7(40):35371-86.
10. Seiti M, Giuri A, Corcione CE, Ferraris E. Advancements in tailoring PEDOT: PSS properties for bioelectronic applications: A comprehensive review. Biomaterials Advances. 2023;154:213655.
11. Tseghai GB, Mengistie DA, Malengier B, Fante KA, Van Langenhove L. PEDOT:PSS-Based Conductive Textiles and Their Applications. Sensors (Basel). 2020;20(7).
12. Gao N, Yu J, Tian Q, Shi J, Zhang M, Chen S, Zang L. Application of PEDOT:PSS and Its Composites in Electrochemical and Electronic Chemosensors. Chemosensors. 2021;9(4):79.

 doi:10.20944/preprints202512.0183.v1

13. Su Z, Jin Y, Wang H, Li Z, Huang L, Wang H. PEDOT:PSS and Its Composites for Flexible Supercapacitors. ACS Applied Energy Materials. 2022;5(10):11915-32.
14. Khasim S, Pasha A, Badi N, Lakshmi M, Mishra YK. Retracted Article: High performance flexible supercapacitors based on secondary doped PEDOT–PSS–graphene nanocomposite films for large area solid state devices. RSC Advances. 2020;10(18):10526-39.
15. Li Y, Ren G, Zhang Z, Teng C, Wu Y, Lu X, et al. A strong and highly flexible aramid nanofibers/PEDOT:PSS film for all-solid-state supercapacitors with superior cycling stability. Journal of Materials Chemistry A. 2016;4(44):17324-32.
16. Li L, Zhang N, Zhang M, Zhang X, Zhang Z. Flexible Ti3C2Tx/PEDOT:PSS films with outstanding volumetric capacitance for asymmetric supercapacitors. Dalton Transactions. 2019;48(5):1747-56.
17. Xue H, Huang P-H, Göthelid M, Strömberg A, Niklaus F, Li J. Ultrahigh-Rate On-Paper PEDOT:PSS-Ti2C Microsupercapacitors with Large Areal Capacitance. Advanced Functional Materials. 2024;34(49):2409210.
18. He W, Wang C, Zhuge F, Deng X, Xu X, Zhai T. Flexible and high energy density asymmetrical supercapacitors based on core/shell conducting polymer nanowires/manganese dioxide nanoflakes. Nano Energy. 2017;35:242-50.
19. Skorupa M, Karoń K, Marchini E, Caramori S, Pluczyk-Małek S, Krukiewicz K, Carli S. PEDOT:Nafion for Highly Efficient Supercapacitors. ACS Applied Materials & Interfaces. 2024;16(18):23253-64.
20. Akbar AR, Saleem A, Rauf A, Iqbal R, Tahir M, Peng G, et al. Integrated MnO2/PEDOT composite on carbon cloth for advanced electrochemical energy storage asymmetric supercapacitors. Journal of Power Sources. 2023;579:233181.
21. Fan Y, Wang T, Asrosa R, Li B, Naresh N, Liu X, et al. Synergistic contribution of activated carbon and PEDOT:PSS in hybrid electrodes for high-performance planar micro-supercapacitors. Chemical Engineering Journal. 2024;488:150672.
22. Park J, Lee A, Yim Y, Han E. Electrical and thermal properties of PEDOT:PSS films doped with carbon nanotubes. Synthetic Metals. 2011;161(5):523-7.
23. Shewale PS, Yun K-S. Ternary nanocomposites of PEDOT: PSS, RGO, and urchin-like hollow microspheres of NiCo2O4 for flexible and weavable supercapacitors. Materials Science and Engineering: B. 2023;292:116404.
24. Brooke R, Franco-Gonzalez JF, Wijeratne K, Pavlopoulou E, Galliani D, Liu X, et al. Vapor phase synthesized poly(3,4-ethylenedioxythiophene)-trifluoromethanesulfonate as a transparent conductor material. Journal of Materials Chemistry A. 2018;6(43):21304-12.
25. Ali M, Lee C, Soh H, Lee J. Effects of the FeCl 3 concentration on the polymerization of conductive poly(3,4-ethylenedioxythiophene) thin films on (3-aminopropyl) trimethoxysilane monolayer-coated SiO 2 surfaces. Metals and Materials International - MET MATER INT. 2009;15:977-81.
26. Ali MA, Kim H, Lee C, Nam H, Lee J. Effects of iron(III) p-toluenesulfonate hexahydrate oxidant on the growth of conductive poly(3,4-ethylenedioxythiophene) (PEDOT) nanofilms by vapor phase polymerization. Synthetic Metals. 2011;161(13):1347-52.
27. Wang K-S, Lan H-T, Wu C-H, Chen Y-C, Lin Y-J, Sung T-J, et al. Electrochemical polymerization of PEDOT:PSS with graphene oxide and silver nanoparticles for antibacterial coating and SERS detection. Surface and Coatings Technology. 2024;485:130889.
28. Wang J, Fang B-S, Chou K-Y, Chen C-C, Gu Y. A two-stage enzymatic synthesis of conductive poly(3,4-ethylenedioxythiophene). Enzyme and Microbial Technology. 2014;54:45-50.
29. Sakunpongpitiporn P, Phasuksom K, Paradee N, Sirivat A. Facile synthesis of highly conductive PEDOT:PSS via surfactant templates. RSC Advances. 2019;9(11):6363-78.
30. Dietlin C, Schweizer S, Xiao P, Zhang J, Morlet-Savary F, Graff B, et al. Photopolymerization upon LEDs: new photoinitiating systems and strategies. Polymer Chemistry. 2015;6(21):3895-912.
31. Tehfe MA, Louradour F, Lalevée J, Fouassier J-P. Photopolymerization Reactions: On the Way to a Green and Sustainable Chemistry. Applied Sciences. 2013;3(2):490-514.
32. Zhou X, Fang S, Hu Y, Du X, Ding H, Chai R, et al. Photoinduced double hydrogen-atom transfer for polymerization and 3D printing of conductive polymer. Nature Synthesis. 2024;3(9):1145-57.
33. Bagheri A, Jin J. Photopolymerization in 3D Printing. ACS Applied Polymer Materials. 2019;1(4):593-611.

 doi:10.20944/preprints202512.0183.v1

34. Baltazar J, Sojoudi H, Paniagua SA, Zhang S, Lawson RA, Marder SR, et al. Photochemical Doping and Tuning of the Work Function and Dirac Point in Graphene Using Photoacid and Photobase Generators. Advanced Functional Materials. 2014;24(32):5147-56.
35. Wochnowski C, Metev S. UV-laser-assisted synthesis of iodine-doped electrical conductive polythiophene. Applied Surface Science. 2002;186(1):34-9.
36. Kaya K. A green and fast method for PEDOT: Photoinduced step-growth polymerization of EDOT. Reactive and Functional Polymers. 2023;182:105464.
37. Tabak T, Kaya K, Isci R, Ozturk T, Yagci Y, Kiskan B. Combining Step-Growth and Chain-Growth Polymerizations in One Pot: Light-Induced Fabrication of Conductive Nanoporous PEDOT-PCL Scaffold. Macromolecular Rapid Communications. 2024;45(2):2300455.
38. Tabak T, Altinisik S, Ulucay S, Koyuncu S, Kaya K. Black-to-Transmissive Electrochromic Switching PEDOT-co-poly(N-ethylcarbazole) via a Sustainable and Facile In Situ Photo(co)polymerization Method. Macromolecules. 2024;57(10):4769-81.
39. Ermis S, Tohtayeva J, Altinisik S, Ulucay S, Jockusch S, Kiskan B, et al. Photopolymerized PEDOT-coated polydopamine: A Green approach for supercapacitor electrode materials. Reactive and Functional Polymers. 2025;216:106414.
40. Nguyen DM, Lo C-Y, Guo T, Choi T, Sundar S, Swain Z, et al. One Pot Photomediated Formation of Electrically Conductive Hydrogels. ACS Polymers Au. 2024;4(1):34-44.
41. Awasthi H, Kumar PS, Thundat T, Goel S. Flexible Supercapacitor Device Based on Laser-Synthesized Nanographene for Low-Power Applications. Advanced Energy and Sustainability Research. 2024;5(12):2400180.
42. Rajeevan S, John S, George SC. Polyvinylidene fluoride: A multifunctional polymer in supercapacitor applications. Journal of Power Sources. 2021;504:230037.
43. Ab. Rahim AH, Ramli N, Nordin AN, Abd. Wahab MF. Supercapacitor performance with activated carbon and graphene nanoplatelets composite electrodes, and insights from the equivalent circuit model. Carbon Trends. 2021;5:100101.
44. Kati M, Cakir YB, Kaya K, Kiliclar HC, Kiskan B. Phenacyl bromide as Norrish type I photoinitiator for the facile synthesis of chain-end functional PMMA and polystyrene. Frontiers in Materials. 2024;Volume 11 - 2024.
45. Li J, Liu J, Gao C, Zhang J, Sun H. Influence of MWCNTs Doping on the Structure and Properties of PEDOT:PSS Films. International Journal of Photoenergy. 2009;2009(1):650509.
46. Song C, Zhong Z, Hu Z, Wang J, Wang L, Ying L, et al. Methanol treatment on low-conductive PEDOT:PSS to enhance the PLED's performance. Organic Electronics. 2016;28:252-6.
47. Lyu D, Jin Y, Magusin PCMM, Sturniolo S, Zhao EW, Yamamoto S, et al. Operando NMR electrochemical gating studies of ion dynamics in PEDOT:PSS. Nature Materials. 2023;22(6):746-53.
48. Kopp SM, Deng J-R, Redman AJ, Gotfredsen H, Jacobs RMJ, Anderson HL, Timmel CR. Cationic polaron delocalization in porphyrin nanoribbons. Chem. 2024;10(12):3595-606.
49. Cho H, Cho W, Kim Y, Lee JG, Kim JH. Influence of residual sodium ions on the structure and properties of poly(3,4-ethylenedioxythiophene):poly(styrenesulfonate). RSC Adv. 2018;8(51):29044-50.
50. Zhang Y, Wang Q, Hu F, Wang Y, Wu D, Wang R, Duhm S. Photoelectron Spectroscopy Reveals the Impact of Solvent Additives on Poly(3,4-ethylenedioxythiophene):poly(styrenesulfonate) Thin Film Formation. ACS Physical Chemistry Au. 2023;3(3):311-9.
51. Thappily P, Shiju K. Enhanced optical and electrical properties of PEDOT:PSS/Gold nanocomposite system. AIP Conference Proceedings. 2014;1620(1):587-91.
52. Wu Z, Wang X, Hou S, Liu Y, Tang Z, Yin L, et al. Scalable and Tunable PEDOT:PSS Emitter for Thermal Camouflage. Advanced Optical Materials. 2024;12(1):2301303.
53. Fan X, Xu B, Liu S, Cui C, Wang J, Yan F. Transfer-Printed PEDOT:PSS Electrodes Using Mild Acids for High Conductivity and Improved Stability with Application to Flexible Organic Solar Cells. ACS Applied Materials & Interfaces. 2016;8(22):14029-36.

 doi:10.20944/preprints202512.0183.v1

54. Say MG, Brett CJ, Edberg J, Roth SV, Söderberg LD, Engquist I, Berggren M. Scalable Paper Supercapacitors for Printed Wearable Electronics. ACS Applied Materials & Interfaces. 2022;14(50):55850-63.
55. Zabihi F, Ahmadian-Yazdi M-R, Eslamian M. Fundamental Study on the Fabrication of Inverted Planar Perovskite Solar Cells Using Two-Step Sequential Substrate Vibration-Assisted Spray Coating (2S-SVASC). Nanoscale Research Letters. 2016;11(1):71.